JACS
JOURNAL OF THE AMERICAN CHEMICAL SOCIETY
Article
pubs.acs.org/JACS

Gas-Phase and Computational Study of Identical Nickel- and Palladium-Mediated Organic Transformations Where Mechanisms Proceeding via M^{II} or M^{IV} Oxidation States Are Determined by Ancillary Ligands

Krista L. Vikse,[†] George N. Khairallah,[†] Alireza Ariafard,*[,†,‡,§] Allan J. Canty,[§] and Richard A. J. O'Hair*[,†]

[†]School of Chemistry, Bio21 Institute of Molecular Science and Biotechnology, University of Melbourne, Parkville, Victoria 3010, Australia

[‡]Department of Chemistry, Faculty of Science, Central Tehran Branch, Islamic Azad University, Shahrak Gharb, Tehran 1467686831, Iran

[§]School of Physical Sciences, University of Tasmania, Hobart, Tasmania 7001, Australia

Supporting Information

ABSTRACT: Gas-phase studies utilizing ion−molecule reactions, supported by computational chemistry, demonstrate that the reaction of the enolate complexes $[(CH_2CO_2—C,O)M(CH_3)]^-$ (M = Ni (**5a**), Pd (**5b**)) with allyl acetate proceed via oxidative addition to give M^{IV} species $[(CH_2CO_2—C,O)M(CH_3)(\eta^1\text{-}CH_2—CH{=}CH_2)(O_2CCH_3—O,O')]^-$ (**6**) that reductively eliminate 1-butene, to form $[(CH_2CO_2—C,O)M(O_2CCH_3—O,O')]^-$ (**4**). The mechanism contrasts with the M^{II}-mediated pathway for the analogous reaction of $[(phen)M(CH_3)]^+$ (**1a,b**) (phen = 1,10-phenanthroline). The different pathways demonstrate the marked effect of electron-rich metal centers in enabling higher oxidation state pathways. Due to the presence of two alkyl groups, the metal-occupied d orbitals (particularly d_{z^2}) in **5** are considerably destabilized, resulting in more facile oxidative addition; the electron transfer from d_{z^2} to the C=C π^* orbital is the key interaction leading to oxidative addition of allyl acetate to M^{II}. Upon collision-induced dissociation, **4** undergoes decarboxylation to form **5**. These results provide support for the current exploration of roles for Ni^{IV} and Pd^{IV} in organic synthesis.

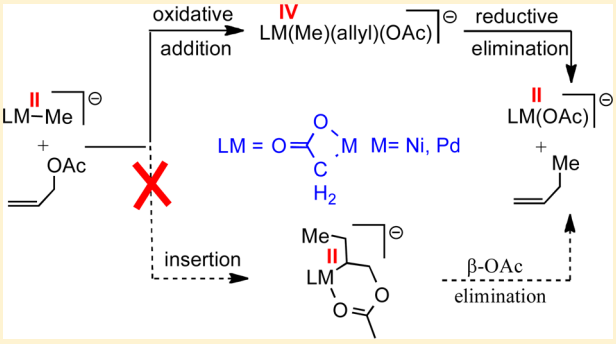

INTRODUCTION

The ability of transition metals to access a range of oxidation states contributes significantly to their flexible roles in metal-mediated organic synthesis. For the group 10 metal nickel, there is now significant evidence from the Sanford laboratory that encourages the search for applications of Ni^{IV} in synthesis,[1] subsequent to earlier suggestions of Ni^{IV} involvement.[2] These advances complement the established roles for the lower oxidation states of nickel[2a] and the +IV oxidation state for its congener palladium.[1,3] For both Ni^{IV} and Pd^{IV}, the stability of these high oxidation state complexes is enhanced by the presence of strongly donating polydentate ligands.[1a,b,3] In view of this, we have explored the possibility of developing reaction sequences involving the same organic transformation but proceeding via M^{II} or M^{IV} species as the ancillary ligand is altered.

The present study follows our recent report of a mass spectrometric examination, in concert with a density functional theory (DFT) exploration of mechanism, for the gas-phase reaction of $[(phen)M(CH_3)]^+$ (M = Ni (**1a**), Pd (**1b**); phen =1,10-phenanthroline) with allyl acetate (Scheme 1).[4−7] This study established that an ion−molecule reaction (IMR) occurs via alkene insertion to give **2** followed by β-acetate elimination and subsequent dissociation of 1-butene to give **3**.

Collision-induced dissociation (CID) of $[(phen)M(O_2CCH_3—O,O')]^+$ (**3**) results in decarboxylation to give **1**,[8,9] which is also the procedure used for the initial synthesis of **1** from **3** that has been prepared via electrospray ionization (ESI) of the metal acetate complex. DFT calculations are supportive of a mechanism involving M^{II} species throughout and exclude the possibility of oxidative addition of allyl acetate as the initial step in a M^{IV}-mediated pathway.[10]

We report here the identification, via gas-phase and DFT studies, of the same organic transformation where phen is replaced by an anionic enolate bidentate group. Interestingly, in this case, the mechanism proceeds via oxidative addition of allyl acetate to $[(CH_2CO_2—C,O)M(CH_3)]^-$ forming a M^{IV}

Received: July 31, 2015
Published: October 15, 2015

DOI: 10.1021/jacs.5b08044
J. Am. Chem. Soc. 2015, 137, 13588−13593

Scheme 1. Gas-Phase and DFT Study of the Reaction of the Ion−Molecule Reaction of Allyl Acetate with $[(phen)M(CH_3)]^+$ (M = Ni (1a), Pd (1b)).[4]

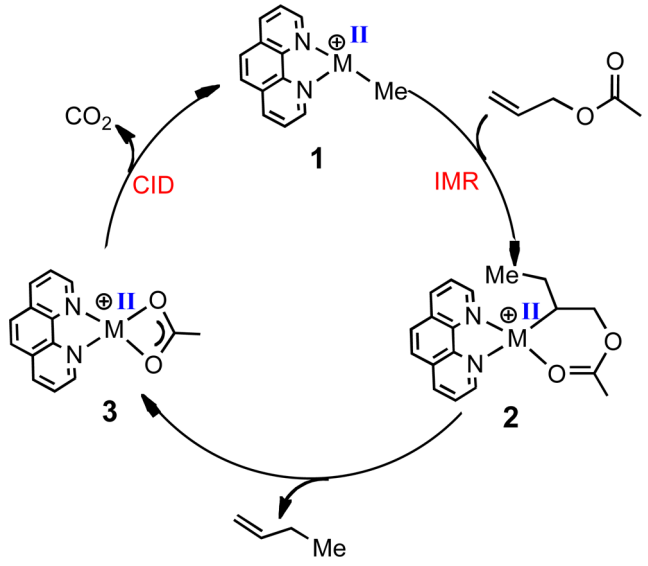

complex that undergoes reductive elimination to give 1-butene and $[(CH_2CO_2—C,O)M(O_2CCH_3—O,O')]^-$ (Scheme 2).

Scheme 2. Mechanism for the Ion−Molecule Reaction of Allyl Acetate with $[(CH_2CO_2—C,O)M(CH_3)]^+$ (M = Ni (5a), Pd (5b)) Involving M^{IV} Intermediates (6) To Give 1-Butene and 4, and CID of 4 To Eliminate CO_2 and Return to 5

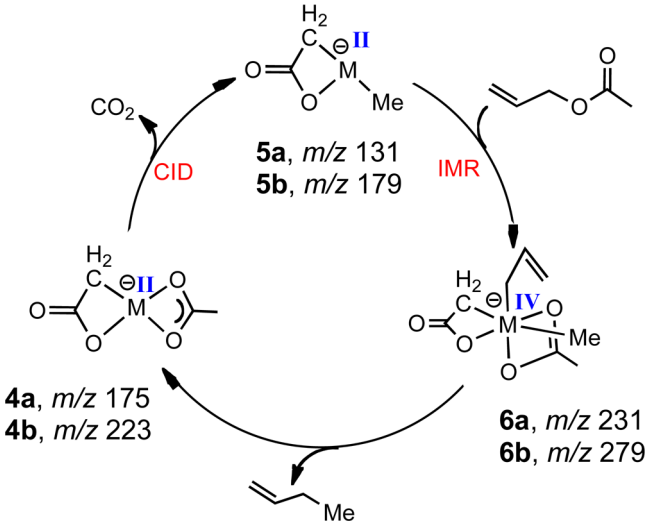

RESULTS AND DISCUSSION

Ion−Molecule Reactions between 5 and Allyl Acetate: Products and Reaction Efficiencies. Metallalactones $[(CH_2CO_2—C,O)M(O_2CCH_3—O,O')]^-$ (M = Ni (**4a**), Pd (**4b**)) were generated under soft electrospray conditions (source voltage ~2.3−2.9 kV) from solutions of the M^{II} acetates in methanol:water (3:1) solutions containing 0.5% acetic acid. The anions (**4**) were mass selected within the linear ion trap mass spectrometer and decarboxylated via CID to form the reactive organometallic anions $[(CH_2CO_2—C,O)M(CH_3)]^-$ (M = Ni (**5a**), Pd (**5b**)). Ion−molecule reactions between mass selected **5** and allyl acetate gives rise to a range of ionic products (Figure 1), including the reformation of **4** via a C−C coupling reaction to give 1-butene.[9]

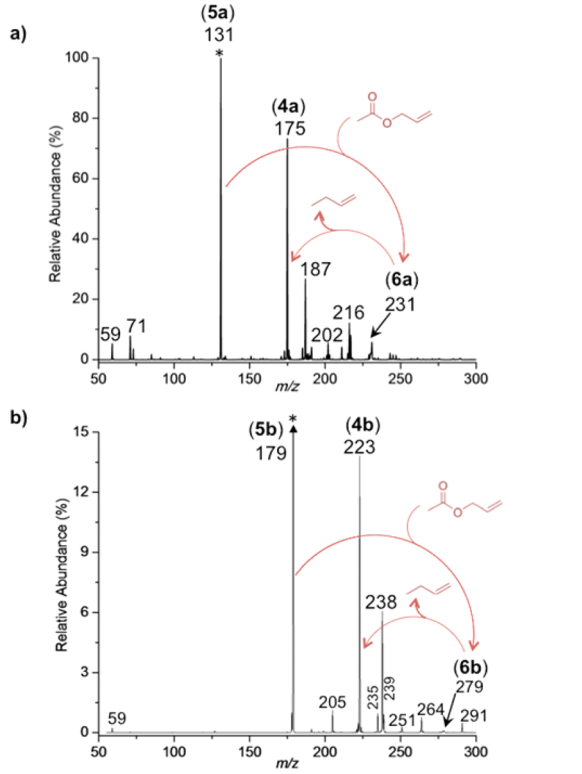

Figure 1. Mass spectra showing ion−molecule reactions between allyl acetate (6×10^{10} molecule/cm^3) and $[(CH_2CO_2—C,O)M(CH_3)]^-$; (a) M = Ni (**5a**) (*m*/*z* 131) giving intermediate **6a** (*m*/*z* 231) and final product **4a** (*m*/*z* 175); (b) M = Pd (**5b**, *m*/*z* 179) giving **6b** (*m*/*z* 279) and **4b** (*m*/*z* 223). Reaction time is 10 s.

The reacting ion is the most intense peak (*m*/*z* 131 (**5a**), 179 (**5b**)), even after exposure to high concentrations of allyl acetate indicating that the reactions of **5** with allyl acetate are slow in the gas phase. Quantitative kinetic experiments (Supporting Information Table S1) confirm that under effectively identical conditions the nickel complex reacts more quickly than the analogous palladium complex: **5a** is consumed nearly an order of magnitude faster (reaction efficiency of 0.14%) than **5b** (reaction efficiency of 0.024%).[11]

Most interestingly, the observed ions **6a** and **6b** have an *m*/*z* value appropriate for M^{II} intermediates analogous to **2** in Scheme 1 *or* the isomeric M^{IV} intermediates $[(CH_2CO_2—C,O)M(CH_3)(\eta^1\text{-}CH_2—CH=CH_2)(O_2CCH_3—O,O')]^-$ (M = Ni (**6a**), Pd (**6b**)). These intermediates are detected in very low abundance for both metal systems. The relative low abundance of these ions can be explained by examining the other observed product signals, which are all indicative of subsequent decomposition processes from the initially formed M^{II} (cf **2**, **3**) or octahedral M^{IV} intermediate (**6**). It is important to note that some of the observed products can only be readily envisaged as arising from an M^{IV} species. Specifically, metal containing anions corresponding to loss of CO_2, butane or acetate may be explained as arising from M^{II} intermediates analogous to **2** or **3**, or M^{IV} intermediates; however, loss of $[CH_2CHCH_2]^\bullet$ or metal-containing anions indicating the loss

DOI: 10.1021/jacs.5b08044
J. Am. Chem. Soc. 2015, 137, 13588−13593

of $CH_3^{\bullet}$, cyclopropene, or $CH_3CO_2CH_3$ necessitate the intermediacy of a M^{IV} species (Scheme 3). An examination of

Scheme 3. Observed Ionic Products of Gas-Phase Ion–Molecule Reactions of Allyl Acetate with $[(CH_2CO_2—C,O)M(CH_3)]^-$ (M = Ni (5a), Pd (5b)), Where the M^{IV} Intermediates (6) Decompose Predominantly via Loss of 1-Butene

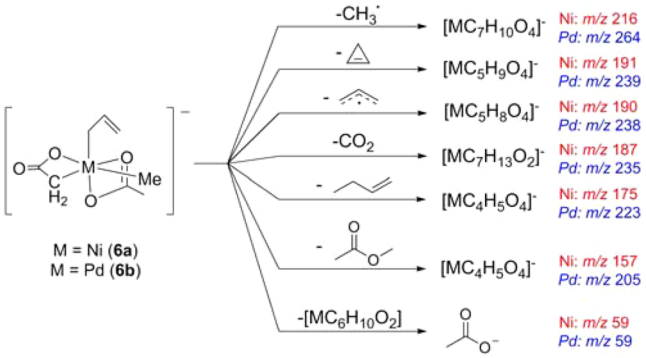

Figure 1 together with a detailed branching ratio analysis (Table S2) for the anions resulting from these seven decomposition routes indicate that formation of 1-butene[12] and **4** is the dominant product pathway, in particular for palladium. Finally, after the ion–molecule reaction, subjecting the isolated product ions **4** to CID results in elimination of CO_2 to reform **5** (Supporting Information Figure S2).

DFT Studies on Mechanisms for Allylic Alkylation of 5 by Allyl Acetate. In the gas phase, the ions **1** or **5** and allyl acetate are attracted to each other by ion–dipole and ion-induced-dipole forces to form the initial complexes **2** and **6**. About 15–20 kcal/mol of energy is typically released in forming the new bonds in these complexes, which is converted into internal energy. The resultant energized complexes can either decompose back to reactants, or if the barrier heights for subsequent reactions are less than the available energy of the energized complexes **2** and **6**, they can proceed to form new products.[13] In DFT studies for the reaction of $[(phen)M(CH_3)]^+$ (**1**) with allyl acetate we reported that barriers (ΔH, relative to the separated reactants) for the oxidative addition/reductive elimination (OA/RE) steps computed as −4.4/+4.7 and −3.9/−4.5 kcal/mol for M = Pd and Ni, respectively, compared with −25.0 and −25.4 kcal/mol for the insertion step (Scheme 1).[4] Because the OA/RE transition structures were substantially higher in energy than the insertion transition structures, the M^{II} pathway is likely to operate.

In commencing our analogous DFT studies of the present system, we note that, for three-coordinate complexes $[(CH_2CO_2—C,O)M(CH_3)]^-$ (**5**), we expect a T-shaped geometry[14] with the strongly donating methyl group to be *cis* to the enolate carbon (**5**) rather than *trans* to the strongly donating enolate carbon (**5′**). Calculations show that **5′** do not correspond to local minima, that is, attempted optimization leads to **5**, but that coordination of allyl acetate allows both *cis* and *trans* isomers of **5′** to be located (Scheme 4).

Each isomer forms three potential linkage isomers: two *O*-bound and one more stable η^2-π bound (**5π_sub**, **5O1_sub**, **5O2_sub**), together with the transition structure for isomerization of the π complex (**5_TS$_{iso}$**), illustrated in Figure 2. All of the *cis*-linkage isomers are computed to be much lower in energy than the *trans*-linkage isomers, for example, 22.9 kcal/

Scheme 4. DFT Exploration of Isomers of Reagents 5 When Coordinated by Allyl Acetate Substrate, sub, Isomerization π-Coordinated Allyl Acetate (5_TS$_{iso}$), and Overview of Pathways Examined for Formation of 1-Butene

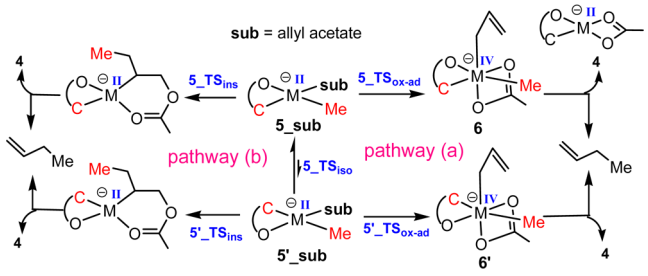

mol for the *O*-bound palladium isomers. However, this energy difference is reduced to 9.9 kcal/mol for the palladium π isomer, where the higher energy isomer, which is more electron-rich at the metal center, benefits from the π-accepting ability of the alkene group. This fact is supported by the longer C=C bond distance in **5b′π_sub** (1.403 Å) than in **5bπ_sub** (1.366 Å) as well as the shorter Pd–alkene bond distances in **5b′π_sub** (2.163 and 2.138 Å) than in **5bπ_sub** (2.315 and 2.346 Å).

The formation of 1-butene through M^{II} and M^{IV} pathways were investigated for both geometrical isomers (Figure 2). The ions **5_TS$_{ins}$** and **5′_TS$_{ins}$** are designated for transition structures of insertion of the alkene into the M^{II}–Me bond of **5_sub** and **5′_sub**, respectively. Figure 2 shows that, for both Ni and Pd systems the most stable transition structures, oxidative addition to **5**[15] and reductive elimination (**6_TS$_{red\text{-}el}$**), all lie below other vital transition structures indicating that the oxidative addition/reductive elimination mechanism for the *cis* isomer is energetically more favorable. Indeed, due to the overall charge of −1 and the presence of two alkyl groups, the metal occupied d orbitals (particularly d_z^2) in **5a** and **5b** are considerably destabilized, resulting in more facile oxidative addition; the electron transfer from d_z^2 to the C=C π^* orbital is the key interaction leading to oxidative addition of allyl acetate to M^{II}. The energies of the HOMO (mainly d_z^2) in **5a**/**5b** are calculated to be −0.66/−1.08 eV, whereas those in **1a**/**1b** are −10.19/−10.29 eV.

Although the strong σ-donating alkyl groups render the metal centers more prone to oxidation, they result in the alkene being weakly coordinated to **5a**/**5b**, and thus all of the transition structures lie above the reference point (separated reactants). For the enolate complexes, this accounts for the slow reaction of **5** with allyl acetate in the gas phase, leading to low reaction efficiencies, 0.14% (Ni) and 0.024% (Pd). Indeed, owing to the lower electron affinity of **5a**/**5b** with respect to **1a**/**1b** as evident from the higher lying LUMO in **5a** (3.24 eV)/**5b** (2.95 eV) than in **1a** (−6.30 eV)/**1b** (−6.55 eV), the enolate complexes are less susceptible to coordination.

Alkene insertion via transition structure **5_TS$_{ins}$** is an unfavorable process because this reaction affords an intermediate in which two strong trans-influencing alkyl ligands occupy trans positions. Also, the instability of adduct **5′_sub** relative to **5_sub** renders all the transition structures connected to this unstable adduct higher in energy than the transition structures of oxidative addition to **5**. The activation barriers for oxidative addition and reductive elimination are lower for nickel, accounting for the higher reactivity of **5a** (reaction efficiency = 0.14%) compared to **5b** (reaction efficiency =

DOI: 10.1021/jacs.5b08044
J. Am. Chem. Soc. 2015, 137, 13588–13593

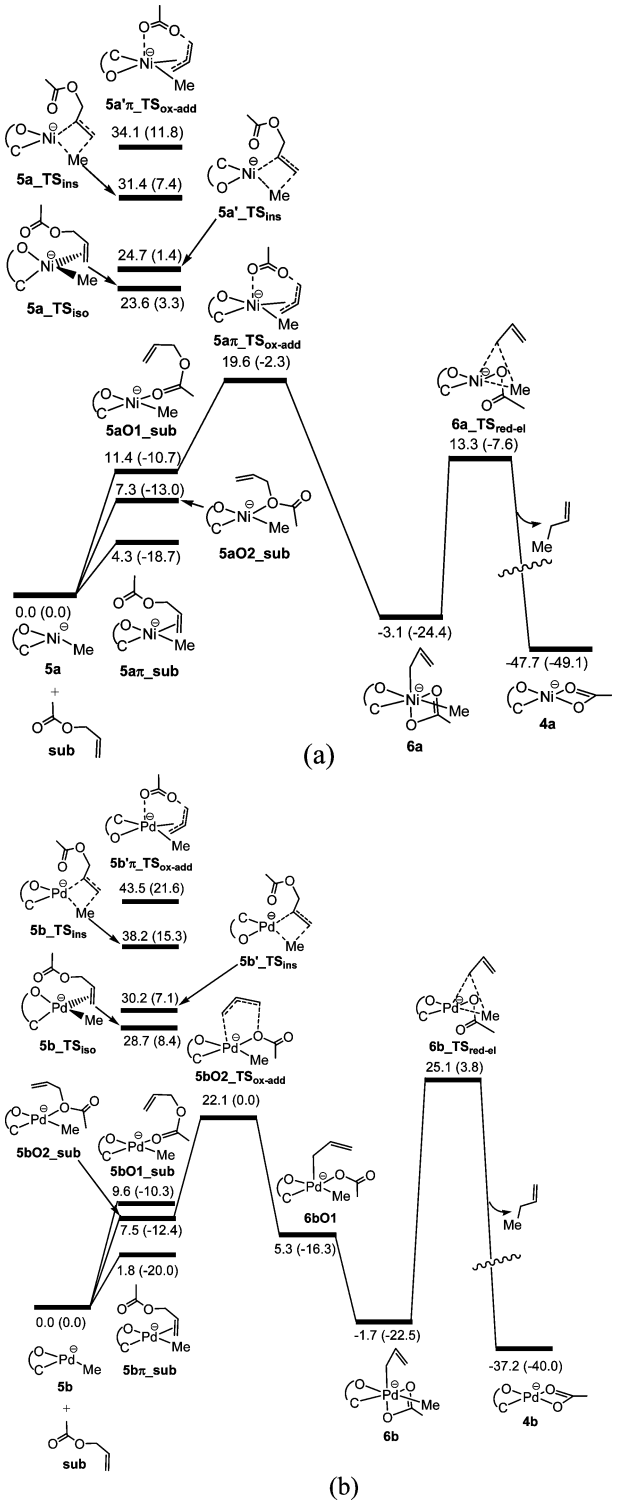

Figure 2. Computed energy profiles for the reaction of $[(CH_2CO_2-C,O)M(CH_3)]^-$ (**5**) with allyl acetate via M^{IV} intermediates to form 1-butene and $[(CH_2CO_2-C,O)M(CH_3CO_2-O,O')]^-$ (**4**). (a) M = Ni; and (b) M = Pd. Computation for the transition structure for isomerization of the π-complex of **5** (**5_TS$_{iso}$**), a high energy M^{IV} transition structure for isomer **5′** (**5′π_TS$_{ox-add}$**) and for the M^{II} pathway (**5_TS$_{ins}$**, **5′_TS$_{ins}$**) are also shown. Energies ΔG (ΔH) are in kcal/mol. Calculations were carried out at the B3LYP-D3BJ level of theory using the basis sets described in the Experimental Section.

0.024%). Finally, we also investigated a transition structure for the palladium case in which, from **5bO1_sub**, a direct coupling between C(allyl) and C(methyl) leads to formation of final product. We found that this transition structure, with a relative Gibbs energy of 48.5 kcal/mol, is much higher in energy than all other transition structures.

On a final note, due to the DFT calculated lower energy of **5bO2_TS$_{ox-add}$** as compared to **6b_TS$_{red-el}$**, the Pd^{IV} intermediate **6b** could be anticipated to be more readily trapped experimentally. A plausible explanation for the low abundance of the intermediate **6b** may be due to the normal errors associated with DFT calculations.[16]

CONCLUSIONS

In conclusion, we find that on the basis of both gas-phase and DFT studies, $[(CH_2CO_2-C,O)M(CH_3)]^-$ (M = Ni (**5a**), Pd (**5b**)) react with allyl acetate under mass spectrometry conditions via M^{IV} intermediates (Scheme 2) to give 1-butene. In contrast, $[(phen)M(CH_3)]^+$ reacts via Pd^{II} species to give the same organic product (Scheme 1). Consistent with established organopalladium(IV) chemistry, and emerging organonickel(IV) chemistry pioneered by Klein[17] and Sanford,[1a,b] the difference in mechanism can be attributed to the higher donor ability of the enolate ligand in the anionic reagents favoring the formation of higher oxidation state species via concerted oxidative addition mechanism.[18] We view the results reported herein as providing timely support for the exploration of roles for Ni^{IV} in organic synthesis and catalysis.

EXPERIMENTAL SECTION

Mass Spectrometry Experiments. In order to allow direct comparisons, gas-phase ion−molecule reactions were conducted in a similar manner to those reported for the reactivity studies of $[(phen)M(CH_3)]^+$.[4] Briefly, palladium(II) acetate or nickel(II) acetate tetrahydrate were dissolved in methanol:water (3:1) containing 0.5% acetic acid to give a 0.5−1.0 mM solution. The solution was transferred via syringe pump operating at 5−10 μL min^{-1} to the electrospray source of a Finnigan LTQ FT hybrid linear ion trap (Finnigan, Bremen, Germany) previously modified to allow the introduction of neutral reagents into the ion trap.[19] Typical ESI, CID, and IMR conditions used are given in the Supporting Information.

DFT Calculations. Gaussian 09[20] was used to fully optimize all the structures reported in this paper at the B3LYP-D3BJ level of theory. The effective-core potential of Hay and Wadt with a double-ξ valence basis set (LANL2DZ) was chosen to describe Ni and Pd. The 6-31G(d) basis set was used for other atoms. Polarization functions were also added for Ni (ξ_f = 3.130) and Pd (ξ_f = 1.472). This basis set combination will be referred to as BS1. Frequency calculations were carried out at the same level of theory as those for the structural optimization. Transition structures were located using the Berny algorithm. Intrinsic reaction coordinate (IRC) calculations were used to confirm the connectivity between transition structures and minima. To further refine the energies obtained from the B3LYP-D3BJ/BS1 calculations, we carried out single-point energy calculations for all of the structures with a larger basis set (BS2). BS2 utilizes the def2-TZVP basis set on all atoms. Effective core potentials including scalar relativistic effects were used for palladium atom

To estimate the corresponding enthalpy, ΔH, and Gibbs energies, ΔG, the corrections were calculated at the B3LYP-D3BJ/BS1 level using the conditions of T = 298.15 K; $P = 2 \times 10^{-3}$ Torr, which reflect the operating conditions of the ion trap

DOI: 10.1021/jacs.5b08044
J. Am. Chem. Soc. 2015, 137, 13588−13593

($T \approx 298$ K; $P \approx 2 \times 10^{-3}$ Torr)[21] and finally added to the single-point energies. We have used the corrected enthalpy and Gibbs free energies obtained from the B3LYP-D3BJ/BS2//B3LYP-D3BJ/BS1 calculations throughout the paper unless otherwise stated.

Minimum energy crossing points (MECPs) between closed-shell singlet and triplet states were located using the code of Harvey et al.[22] and used to estimate the reaction barrier of the radical mechanism (Supporting Information Figure S3).[18] Because the MECPs do not correspond to stationary points, their energies are reported uncorrected.

■ ASSOCIATED CONTENT

Supporting Information

The Supporting Information is available free of charge on the ACS Publications website at DOI: 10.1021/jacs.5b08044.

Cartesian coordinates of species examined by DFT, a full citation of ref 20, and details of mass spectrometry experimentation and computational approaches. (PDF)

■ AUTHOR INFORMATION

Corresponding Authors

*rohair@unimelb.edu.au

*Alireza.Ariafard@utas.edu.au

Notes

The authors declare no competing financial interest.

■ ACKNOWLEDGMENTS

We thank the ARC for financial support via grant DP110103844 (to R.A.J.O. and G.N.K.), DP1096134 (to G.N.K.), DP120101540 (A.J.C.), DP150101388 (A.J.C. and R.A.J.O.) and through the ARC CoE program. The authors gratefully acknowledge the generous allocation of computing time from the University of Tasmania and the National Computing Infrastructure.

■ REFERENCES

(1) (a) Camasso, N. M.; Sanford, M. S. *Science* **2015**, *347*, 1218. (b) Bour, J. R.; Camasso, N. M.; Sanford, M. S. *J. Am. Chem. Soc.* **2015**, *137*, 8034. (c) Riordan, C. G. *Science* **2015**, *347*, 1203. (d) Mitra, R.; Pörschke, K.-R. *Angew. Chem., Int. Ed.* **2015**, *54*, 7488.

(2) (a) Tasker, S. Z.; Standley, E. A.; Jamison, T. F. *Nature* **2014**, *509*, 299. (b) Montgomery, J. In *Organometallics in Synthesis: Fourth Manual*; Lipshultz, B. H., Ed.; Wiley: Hoboken, NJ, 2013; pp 319–428. (c) Terao, J.; Kambe, N. *Acc. Chem. Res.* **2008**, *41*, 1545. (d) Aihara, Y.; Chatani, N. *J. Am. Chem. Soc.* **2014**, *136*, 898.

(3) (a) Canty, A. J. *Acc. Chem. Res.* **1992**, *25*, 83. (b) Canty, A. J. *Dalton Trans.* **2009**, 10409. (c) Xu, L.-M.; Li, B.-J.; Yang, Z.; Shi, Z.-J. *Chem. Soc. Rev.* **2010**, *39*, 712. (d) Sehnal, P.; Taylor, R. J. K.; Fairlamb, I. J. S. *Chem. Rev.* **2010**, *110*, 824.

(4) Woolley, M.; Ariafard, A.; Khairallah, G. N.; Kwan, K H.-J.; Donnelly, P. S.; White, J. M.; Canty, A. J.; Yates, B. F.; O'Hair, R. A. J. *J. Org. Chem.* **2014**, *79*, 12056.

(5) For other reports of metal catalyzed decarboxylative allylation reactions of allyl acetate, see (a) Rijs, N. J.; O'Hair, R. A. J. *Organometallics* **2012**, *31*, 8012. (b) Al Sharif, H.; Vikse, K. L.; Khairallah, G. N.; O'Hair, R. A. J. *Organometallics* **2013**, *32*, 5416. (c) O'Hair, R. A. J. *Pure Appl. Chem.* **2015**, *87*, 391.

(6) Decarboxylative allylation reactions have been widely explored in the condensed phase; see (a) Burger, E. C.; Tunge, J. A. *J. Am. Chem. Soc.* **2006**, *128*, 10002. (b) Weaver, J. D.; Recio, A.; Grenning, A. J.; Tunge, J. A. *Chem. Rev.* **2011**, *111*, 1846.

(7) For reviews of organonickel chemistry in the gas phase, see (a) Mó, O.; Yáñez, M.; Salpin, J.-Y.; Tortajada, J. *Mass Spectrom. Rev.* **2007**, *26*, 474. (b) Schwarz, H.; Schlangen, M. *J. Catal.* **2011**, *284*, 126.

(8) The use of CID to form organometallic ions via decarboxylation of metal carboxylate ions has been recently reviewed; see O'Hair, R. A. J.; Rijs, N. J. *Acc. Chem. Res.* **2015**, *48*, 329.

(9) There are two potential sites of decarboxylation of **4a** and **4b**: the acetate ligand or the enolate ligand. Detailed labeling studies and DFT calculations have shown that the major site of decarboxylation is the acetate ligand to give **5a** and **5b**; see Vikse, K. L.; Khairallah, G. N.; O'Hair, R. A. J. *Organometallics* **2012**, *31*, 7467.

(10) Sawamura has discussed the mechanistic possibilities for metal catalyzed allylation reactions of allylic esters; see (a) Ohmiya, H.; Makida, Y.; Tanaka, T.; Sawamura, M. *J. Am. Chem. Soc.* **2008**, *130*, 17276. (b) Ohmiya, H.; Makida, Y.; Li, D.; Tanabe, M.; Sawamura, M. *J. Am. Chem. Soc.* **2010**, *132*, 879. (c) Li, D.; Tanaka, T.; Ohmiya, H.; Sawamura, M. *Org. Lett.* **2010**, *12*, 3344. (d) Makida, Y.; Ohmiya, H.; Sawamura, M. *Chem. - Asian J.* **2011**, *6*, 410.

(11) We isolated the ions at m/z 179 (**5b**) after a 10 s reaction time and subjected this to a subsequent 10 s reaction period. The resulting spectrum (Supporting Information Figure S1) was nearly identical to that obtained after the first reaction period, indicating that the remaining signal at m/z 179 in Figure 1b does not represent an unreactive form of **5b**.

(12) The neutral products of ion–molecule reactions are not detected and cannot be characterized in our experiments because they have no charge and cannot be trapped in the ion trap mass spectrometer. For rare examples of the isolation and characterization of neutral products of gas-phase ion–molecule reactions using "one-of-a-kind" instrumentation, see (a) Smith, M. A.; Barkley, R. M.; Ellison, G. B. *J. Am. Chem. Soc.* **1980**, *102*, 6851. (b) Jones, M. E.; Kass, S. R.; Filley, J.; Barkeley, R. M.; Ellison, G. B. *J. Am. Chem. Soc.* **1985**, *107*, 109.

(13) (a) Garver, J. M.; Fang, Y.-R.; Eyet, N.; Villano, S. M.; Bierbaum, V. M.; Westaway, K. C. *J. Am. Chem. Soc.* **2010**, *132*, 3808. (b) De Puy, C. H. *J. Org. Chem.* **2002**, *67*, 2393.

(14) For a review of T-shaped group 10 metal complexes, see Ortuño, M. A.; Conejero, S.; Lledós, A. *Beilstein J. Org. Chem.* **2013**, *9*, 1352.

(15) Different types of oxidative addition transition structures were located. For clarity, the most stable transition structures are depicted in Figure 2, and all others are given in Supporting Information Figure S4.

(16) Preliminary single point calculations at the CCSD(T)/BS3 level supports this possibility (BS3 utilizes SDD with ECP for Pd and 6-31G(d,p) for the other atoms). The CCSD(T) calculated Gibbs energies show that although the oxidative addition barrier **5bO2_TS**$_{\text{ox-add}}$, (25.3 kcal/mol) remains less than **5b_TS**$_{\text{iso}}$ and **5b_TS**$_{\text{ins}}$ (by 3.0 and 8.3 kcal/mol, respectively), it is higher in energy than **6b_TS**$_{\text{red-el}}$ (by 4.1 kcal/mol). This not only highlights the operation of the Pd^{IV} pathway but also explains why **6b** is not readily trapped experimentally, and thus represents a minor product ion in the mass spectrum (Figure 1b).

(17) Klein, H.-F.; Bickelhaupt, A.; Jung, T.; Cordier, G. *Organometallics* **1994**, *13*, 2557.

(18) A radical mechanism via single electron transfer (SET) from the M d_z^2 orbital to the C—O ester σ^* orbital provides an alternative pathway to the formation of **6**. The calculations show that the first step of this mechanism by which allyl and M^{III} radicals are formed is extremely energy consuming due to the fact that the C—O σ bond is relatively strong. The MECP energies between the closed shell singlet and triplet states for the Ni and Pd systems are calculated to lie 23.7 and 32.2 kcal/mol above oxidative addition transition structures **5a**π**_TS**$_{\text{ox-add}}$ and **5bO2_TS**$_{\text{ox-add}}$, respectively (Supporting Information Figure S3). This result suggests that the radical mechanism does not operate (for details see the discussion in the Supporting Information). We thank a reviewer for suggesting this alternative mechanism.

(19) Donald, W. A.; McKenzie, C. J.; O'Hair, R. A. J. *Angew. Chem., Int. Ed.* **2011**, *50*, 8379.

DOI: 10.1021/jacs.5b08044
J. Am. Chem. Soc. 2015, 137, 13588–13593

(20) Frisch, M. J. et al. *Gaussian 09*, Revision D.01; Gaussian, Inc.: Wallingford, CT, 2009.
(21) Donald, W. A.; Khairallah, G. N.; O'Hair, R. A. J. *J. Am. Soc. Mass Spectrom.* **2013**, *24*, 811.
(22) Harvey, J. N.; Aschi, M.; Schwarz, H.; Koch, W. *Theor. Chem. Acc.* **1998**, *99*, 95.

DOI: 10.1021/jacs.5b08044
J. Am. Chem. Soc. 2015, 137, 13588−13593